

## Structure and Function of the Conserved 690 Hairpin in *Escherichia coli* 16 S Ribosomal RNA. II.† NMR Solution Structure

Svetlana V. Morosyuk<sup>1</sup>, Philip R. Cunningham<sup>2</sup> and John SantaLucia Jr<sup>1\*</sup>

<sup>1</sup>Department of Chemistry  
Wayne State University  
Detroit, MI 48202, USA

<sup>2</sup>Department of Biological  
Sciences, Wayne State  
University, Detroit  
MI 48202, USA

The solution structure of the conserved 690 hairpin from *Escherichia coli* 16 S rRNA was determined by NMR spectroscopy. The 690 loop is located at the surface of the 30 S subunit in the platform region and has been implicated in interactions with P-site bound tRNA, E-site mRNA, S11 binding, IF3 binding, and in RNA-RNA interactions with the 790 loop of 16 S rRNA and domain IV of 23 S rRNA. The structure reveals a novel sheared type G690·U697 base-pair with a single hydrogen bond from the G690 amino to U697-04. G691 and A696 also form a sheared pair and U692 forms a U-turn with an H-bond to the A695 non-bridging phosphate oxygen. The sheared pairs and U-turn result in the continuous single-stranded stacking of five residues from 6693 to U697 with their Watson-Crick functional groups exposed in the minor groove. The overall fold of the 690 hairpin is similar to the anticodon loop of tRNA. The structure provides an explanation for chemical protection patterns in the loop upon interaction with tRNA, the 50 S subunit, and S11. *In vivo* genetic studies demonstrate the functional importance of the motifs observed in the solution structure of the 690 hairpin.

© 2001 Academic Press

\*Corresponding author

Keywords: NMR; rRNA; 690 loop; 30 S subunit; instant evolution

### Introduction

An impressive amount of structural information on the ribosome has recently become available. Crystal structures of the 70 S ribosome (Cate *et al.*, 1999), individual subunits (Ban *et al.*, 1999, 2000; Clemons *et al.*, 1999; Schluenzen *et al.*, 2000; Wimberly *et al.*, 2000), and rRNA-protein complexes (Agalarov *et al.*, 2000; Nikulin *et al.*, 2000) and three-dimensional cryo-electron microscopy (Frank & Agrawal, 2000; Mueller *et al.*, 2000) are being solved at increasingly higher resolution. In addition, NMR has provided atomic-resolution structures of ribosomal proteins (Berglund *et al.*, 1997; Jaishree *et al.*, 1996; Markus *et al.*, 1998), factors (Battiste *et al.*, 2000; Hard *et al.*, 2000), and several rRNA pieces (Dallas & Moore, 1997; Fountain *et al.*, 1996; Fourmy *et al.*, 1998; Heus & Pardi, 1991; Huang *et al.*, 1996; Szewczak & Moore, 1995).

Here, we present the NMR solution structure of the 690 hairpin of *Escherichia coli* 16 S rRNA. The 690 loop terminates helix 23b in the central domain of the 16 S rRNA and is highly conserved in all three phylogenetic domains (Morosyuk *et al.*, 2000, 2001; Van de Peer *et al.*, 1999). It is located in the platform region of the small subunit and protrudes into the subunit interface with its minor groove nucleotides available for interactions (Cate *et al.*, 1999; Clemons *et al.*, 1999; Merryman *et al.*, 1999b). The 690 loop and the adjacent internal loop are protected from chemical modification by proteins S11 and IF3 (Agalarov & Williamson, 2000; Moazed *et al.*, 1995; Muralikrishna & Wickstrom, 1989; Powers & Noller, 1995; Wickstrom *et al.*, 1986). These data are consistent with the placement of the 690 loop in the 30 S platform, since IF3 and S11 have also been localized at the small subunit platform by electron microscopy and neutron diffraction (McCutcheon *et al.*, 1999; Pon *et al.*, 1982; Stoffler-Meilicke & Stoffler, 1987). The 690 loop has also been implicated in subunit association based on the hydroxyl radical protection of the loop nucleotides (Merryman *et al.*, 1999b). The 70 S ribo-

†Paper I in this series is Morosyuk *et al.* (2000).

E-mail address of the corresponding author:  
jsl@chem.wayne.edu

some crystal structure shows that the 690 loop forms one of the RNA-RNA bridges (bridge B7) with the large subunit (Cate *et al.*, 1999). Footprinting studies indicate that protein S11 protects helix 23b, which suggests a possible interaction between S11 and the 690 loop (Mueller *et al.*, 1997; Powers & Noller, 1995; Stern *et al.*, 1988). Figure 1(a) shows sites of chemical protection and crosslinking of the 690 loop. The 690 loop may also interact with P-site bound tRNA as evidenced by protection from chemical modification by P-site bound tRNA (Moazed & Noller, 1986, 1990), cleavage by hydroxyl radicals generated from the modified 3' end of the tRNA anticodon stem loops at the P-site (Joseph & Noller, 1996; Joseph *et al.*, 1997), and cross links to tRNA (Doring *et al.*, 1994; Osswald *et al.*, 1995; Rinke-Appel *et al.*, 1995). Loop nucleotides G693 and A694 effect binding of the antibiotics pactamycin and edeine, which inhibit initiation of protein synthesis (Egebjerg & Garrett, 1991; Mankin, 1997; Oehler *et al.*, 1997; Woodcock *et al.*, 1991). The A694G mutation confers pactamycin resistance (Mankin, 1997), suggesting that the 690 hairpin loop may be involved in pactamycin binding. Tetracycline derivatives with tethered photo-activated moieties crosslink to positions

G693, G1300 and G1338 of 16 S rRNA, suggesting that these residues form a tetracycline-binding site on the 30 S subunit (Oehler *et al.*, 1997).

Here, we present the NMR solution structure of the 690 loop. The structure reveals novel hydrogen bonding and stacking interactions in the loop. The loop architecture explains the reactivity of the 690 loop nucleotides toward chemical probes and provides insight into the function of the 690 loop. Analysis of alternative functional 690 loop sequences using instant evolution (see the accompanying paper, Morosyuk *et al.*, 2001) indicates that the structural motifs observed in the NMR structure are important for ribosome function *in vivo*.

## Results

### Sequence design

The sequence of the loop and stem of the 14 nucleotide RNA hairpin (14mer) studied by NMR (Figure 1(b)) is identical with residues 688 through 699 of *E. coli* 16 S rRNA, with the exception of an extra G-C base-pair added to stabilize the stem of the hairpin. We recently demonstrated that pairing between residues 688 to 699 and between 689 to 698 is important for ribosome function (Morosyuk *et al.*, 2000). NMR studies were also performed on a 31 nucleotide RNA with the wild-type *E. coli* sequence of residues 680 to 710 of 16 S rRNA (wt31mer) (Morosyuk *et al.*, 2000). It was found that the wt31mer has the same characteristic imino-proton chemical shifts and NOEs as the 14mer model of the 690 hairpin and therefore both molecules form the same hairpin structure. Therefore, addition of an extra G-C pair at the end of the 690 hairpin stem does not appear to affect the loop conformation.

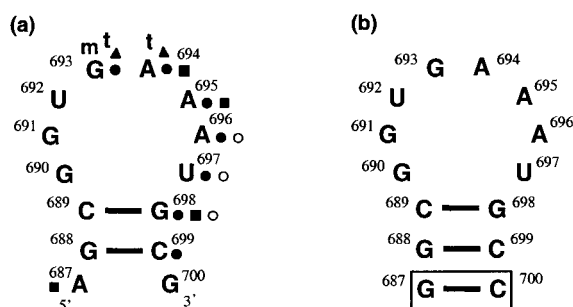


**Figure 1.** (a) Patterns of the base-specific and hydroxyl radical protection of the 690 hairpin in *E. coli* 16 S rRNA. Positions 687 and 700 are not paired in the wild-type sequence, but are a part of the adjacent internal loop. Filled circles (●) indicate sites of the phosphate backbone that are protected from hydroxyl radical cleavage upon association with the 50 S subunits (Merryman *et al.*, 1999b). Open circles (○) indicate sites of hydroxyl radical footprinting of ribosomal protein S11 (Powers & Noller, 1995). Filled squares (■) indicate base-specific footprinting of S11 (Stern *et al.*, 1988). Bold letter t (t) indicates nucleotides crosslinked and/or protected from chemical modifications by P-site bound tRNA (Doring *et al.*, 1994; Joseph *et al.*, 1997; Moazed & Noller, 1986, 1990; Osswald *et al.*, 1995; Rinke-Appel *et al.*, 1995). Filled triangles (▲) indicate nucleotides implicated in antibiotic binding (Egebjerg & Garrett, 1991; Mankin, 1997; Oehler *et al.*, 1997; Woodcock *et al.*, 1991). Bold letter m (m) indicates the site of crosslinking to mRNA (Wollenzien *et al.*, 1991). (b) The 14 nucleotide sequence used in structural studies. The boxed nucleotides were mutated to facilitate isotope labeling by *in vitro* transcription and to thermodynamically stabilize the stem to minimize fraying artifacts.

### Assignment of the base and H1' protons

Initial assignments of the base H6/H8 and sugar H1' and H2' resonances were made based upon 2D NOESY, DQF-COSY and TOCSY experiments of the unlabeled 14mer RNA sample. Adenine H2 chemical shift assignments were confirmed by the long  $T_1$  relaxation time of the H2 protons as well as natural abundance ( $^{13}\text{C}$ ,  $^1\text{H}$ ) HMQC (data not shown) (Varani & Tinoco, 1991). The sequential 2D NOESY walk is shown in Figure 2. At 500 ms mixing time, the base to H1' NOE connectivity is continuous throughout the helix and loop residues except for a missing U692-H1' to G693-H8 cross-peak. Assignments of G693, A694, and A695, however, were initially perplexing due to the connectivity pathway break between U692 and G693, unusual cross-peaks from U692-H1' to A694-H8 and A695-H8, and the atypical upfield shift of the A695-H1' resonance at 4.74 ppm. Unambiguous assignment of these residues was accomplished using a uniformly  $^{13}\text{C}$ ,  $^{15}\text{N}$ -labeled 14mer sample and heteronuclear NMR techniques. A 2D HcCH-

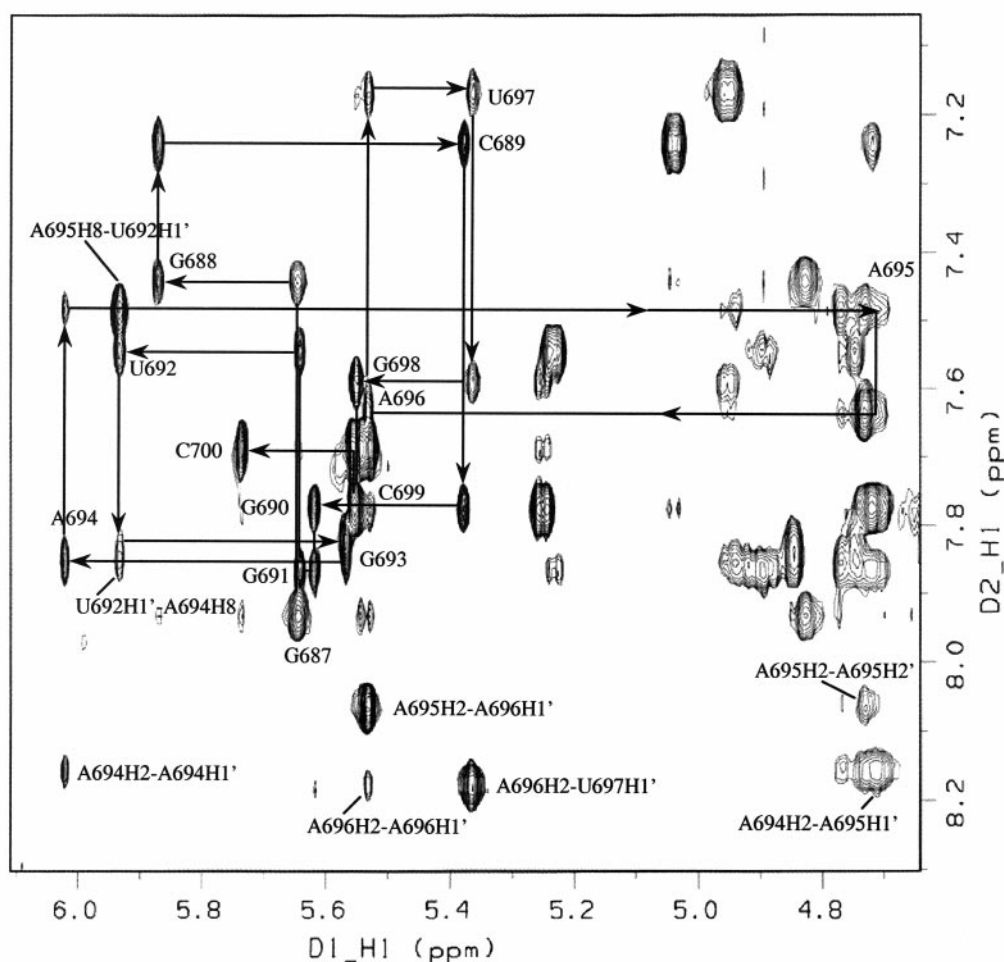


**Figure 2.** Base H8/H6 to H1'/H5 region of the 2D  $^2\text{H}_2\text{O}$  NOESY collected at 15°C and 500 ms mixing time. The sequential walk is shown by arrows. Note the key non-sequential NOEs from A695-H8 to U692-H1' and from A694-H8 to U692-H1' that are characteristic of a U-turn (Stallings & Moore, 1997). Also note the shifted A695-H1' at 4.74 ppm, which indicates that A695-H1' is stacked on the A694 base. Intense cross-peaks are observed between adenine ( $n$ ) H2 to ( $n + 1$ ) H1' for residues A694, A695, and A696.

TOCSY experiment allowed assignment of the H2 and H8 of each adenine (Marino *et al.*, 1994). The 3D HMQC-NOESY confirmed H1' and H2 assignments. All three adenine H2 protons showed strong NOE cross-peaks with H1' of the ( $n + 1$ ) residue in the sequence indicating continuous stacking of the loop bases from A694 to U697 (Figure 2). Non-sequential NOEs from U692-H1' to A694-H8 and A695-H8 provided information about the loop tertiary structure (Figure 2).

#### Assignment of the phosphorus sugar proton and carbon resonances

The sugar proton and carbon resonances were assigned using 2D and 3D heteronuclear NMR techniques on a uniformly  $^{13}\text{C}$ ,  $^{15}\text{N}$ -labeled 14mer RNA molecule (Nikonowicz & Pardi, 1992, 1993; Pardi, 1995). 3D HMQC-NOESY, and 2D and 3D hCCH-TOCSY were used to assign sugar and base carbon atoms. Next, 2D slices through the carbon chemical shifts were used to assign and confirm

the sugar protons from 3D HCCH-COSY, 3D HCCH-TOCSY, and 2D  $^{31}\text{P}$ -decoupled DQF-COSY experiments. Phosphorus resonance assignments were made by the  $^{31}\text{P}$ ,  $^1\text{H}$  HETCOR shown in Figure 3.

#### Assignment of the solvent-exchangeable protons

Imino proton resonances were assigned from 1D NOE difference spectra and 2D NOESY with WATERGATE solvent suppression (Morosyuk *et al.*, 2000). In addition, G and U imino protons were distinguished by their attached  $^{15}\text{N}$  chemical shifts by natural abundance  $^1\text{H}$ ,  $^{15}\text{N}$ -gradient-HMQC (data not shown) (Szewczak *et al.*, 1993). At low temperature, all five imino protons from the loop nucleotides were observed in the 10-12 ppm region of the 1D  $^1\text{H}$  NMR spectra (Figure 4), including two resonances at 11.45 ppm from overlapped U692 and U697 imino proton peaks. The U692 imino proton resonance was

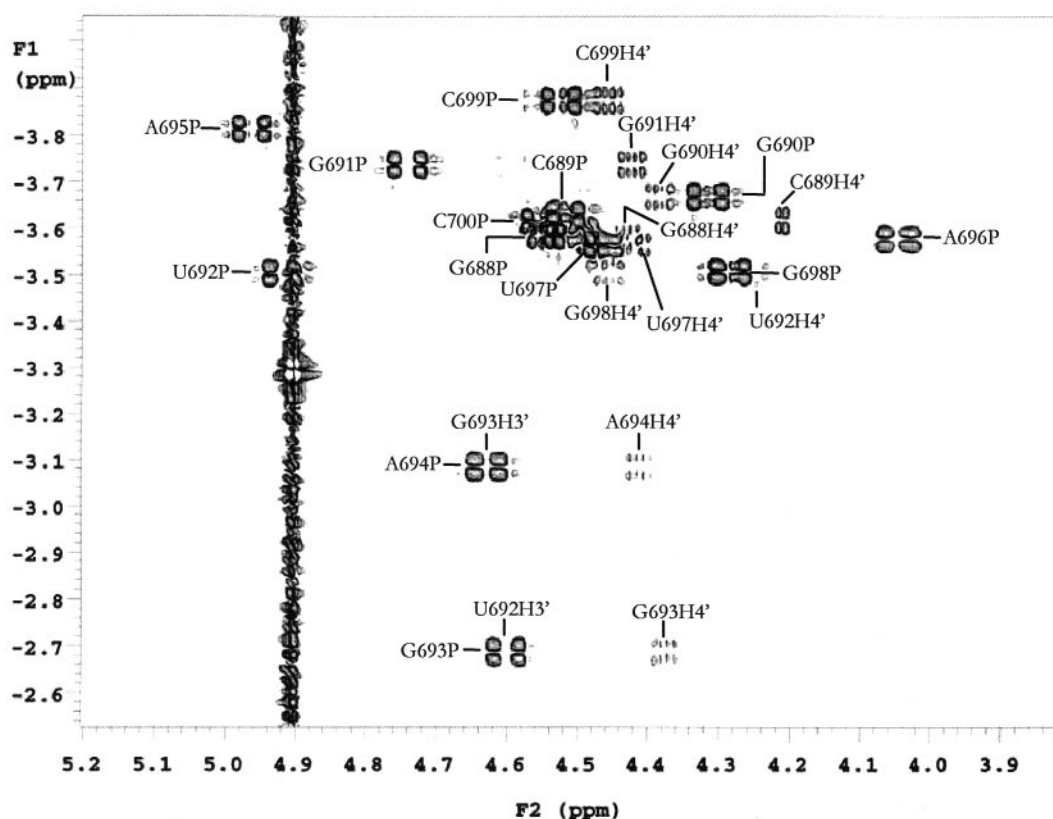


**Figure 3.** 2D  $^{31}\text{P}$ - $^1\text{H}$  HETCOR spectrum. Two shifted  $^{31}\text{P}$  resonance were observed for A694 and G693 residues at  $-2.69$  and  $-3.08$ , respectively, indicating an unusual magnetic environment or *trans* conformation of  $\alpha$  and/or  $\zeta$  torsion angles.  $^{31}\text{P}$ - $\text{H}4'$  four-bond coupling was observed for all residues except A696 and A695 indicating that the other residues are in a "W" conformation (Altona, 1982). P to  $\text{H}5'$  and  $\text{H}5''$   $J$ -couplings are very weak, indicating three-bond  $J$ -coupling less than 3 Hz and therefore indicating  $\beta$  dihedral angles close to  $180^\circ$ .

distinguished from the U697 resonance based upon weak NOEs from the sharp U692 imino proton to A694-H8 and A695-H8 (Figure 5). This is consistent with the 2D  $^2\text{H}_2\text{O}$  NOESY data (Figure 2), which show non-sequential NOEs from U692-H1' to A694-H8 and A695-H8. Therefore, the sharp resonance at 11.45 ppm is from U692 imino proton and the broadened shoulder peak at  $\sim 11.46$  ppm is from the U697 imino proton. These assignments are also consistent with the weak NOEs from the stem G698 imino proton at 13.05 ppm to peaks at 11.46 and 10.78 ppm that are assigned to U697 and G690 (Figure 5) (Morosyuk *et al.*, 2000). Note the absence in Figure 5 of an NOE between G690 and U697. This indicates that G690 and U697 do not form a wobble structure.

The imino protons of G691 and G693 were assigned based upon key NOEs to non-exchangeable protons. G691-H1 shows NOEs to A695-H8 and A696-H8 (Figure 5). The G693-H1 at 10.3 ppm is observed in the 1D NMR spectrum (Figure 4, bottom), but is not observed in the 2D  $\text{H}_2\text{O}$  NOESY spectrum due to broadening from solvent exchange. In the 1D NOE difference spectrum (Figure 4, top), irradiation of the broad G693 imino resonance results in a strong NOE to the A694-H2 resonance at 8.14 ppm and a medium NOE to

A694-H1' at 6.1 ppm. These data indicate that G693 is stacked upon A694.

### Torsion angles

In the short mixing time NOESY spectra, all residues show weak intra-residue NOEs from H8/H6 to H1' (Figure 2) and strong NOEs from H8/H6 to H3'. Therefore, all bases in the 690 loop are in the *anti* conformation. For all residues, very weak or no H1' to H2' cross-peaks were observed in the DQF-COSY spectrum. Therefore,  $J_{\text{H}1'-\text{H}2'}$  couplings are less than 2 Hz, which indicates C3'-endo sugar puckers for all residues (Hall, 1995; Varani *et al.*, 1996). The H1'-H2'  $J$ -couplings were accurately measured by 2D and 3D HCcH E-COSY (Schwalbe *et al.*, 1994).

Backbone dihedral angles involving phosphorus,  $\alpha$ ,  $\beta$ ,  $\epsilon$ , and  $\zeta$  were determined primarily from the 2D ( $^{31}\text{P}$ ,  $^1\text{H}$ ) HETCOR experiment (Figure 3).  $^{31}\text{P}$  chemical shifts for 11 out of 13 residues were found in the narrow region between  $-3.5$  and  $-3.9$  ppm. Nonetheless, unambiguous assignment for all  $^{31}\text{P}$  resonances was possible because of the excellent dispersion of the H3' resonances.  $^{31}\text{P}$  chemical shifts for G693 and A694 are at  $-2.69$  and  $-3.08$  ppm, respectively, indicating an unusual

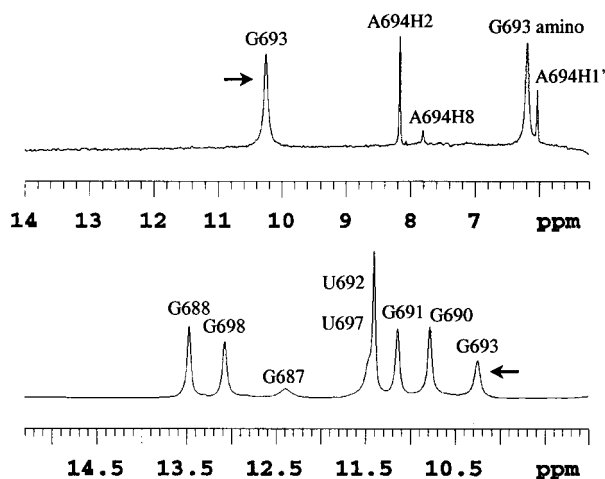


**Figure 4.** Top, 1D NOE difference NMR spectrum at 1°C of the 690 hairpin for G693. Several NOEs are observed (labeled) that resulted from selective irradiation of the G693 resonance (arrow). These novel NOEs were crucial in establishing the fold of the hairpin. Bottom, Imino proton region of the 690 hairpin. Loop resonances are observed between 10 and 12 ppm. The U697 imino resonance at 11.46 ppm is broadened due to solvent exchange and forms a shoulder next to the sharp U692 peak. The 17 Hz linewidth of the U692 peak suggests it is hydrogen bonded, consistent with a U-turn conformation.

magnetic environment or the formation of the unusual *trans* conformation of  $\alpha$  and/or  $\zeta$  torsion angles for these residues (Gorenstein, 1984). Therefore,  $\alpha$  and  $\zeta$  torsion angles were restrained in the calculations to a range of  $0 (\pm 120)^\circ$  for all residues with the exception of G693, A694, and A695, which were unrestrained (see Materials and Methods). Three-bond P-H3' *J*-couplings of 8–12 Hz were measured for all residues, which indicates  $\epsilon$  angles of  $-155 (\pm 30)^\circ$ . In addition, intra-residue four-bond phosphorus to H4' cross-peaks were observed for all residues in the  $^{31}\text{P}$ - $^1\text{H}$  HETCOR of the 14mer (Figure 3) except for A695 and A696. These four-bond couplings indicate a "W" shaped conformation between P and H4' atoms and therefore *trans*  $\beta$  and *gauche*<sup>+</sup>  $\gamma$  angles (Altona, 1982; Lankhorst *et al.*, 1984). Therefore, restraints of  $180 (\pm 30)^\circ$  for  $\beta$  and  $60 (\pm 20)^\circ$  for  $\gamma$  were assigned for all residues except A695 and A696, which were unrestrained. These restraints are supported by weak intra-residue P to H5' and H5'' *J*-couplings and by weak NOEs from base H6/H8 to H5' and H5''.

The H3'-H4' splitting observed in the DQF-COSY cross-peak for A695 is 16 Hz due to the active coupling of  $\sim 8$  Hz and passive H4'-H5'/H5'' coupling of  $\sim 8$  Hz that is characteristic of *trans* or *gauche*<sup>-</sup>  $\gamma$  conformers. Therefore, the A695  $\gamma$  was left unrestrained. A695  $\gamma$  in the *trans* or *gauche* conformation is also consistent with the strong NOEs observed from A695-H8 to A695-H5' and A695-H5'' in 2D  $^2\text{H}_2\text{O}$  NOESY (data not

**Table 1.** NMR distance and dihedral angle constraints

Hydrogen bond restraints <sup>a</sup>	9
Total NOE distance restraints	193
Intra-residue	53
Inter-residue	140
Mean NOEs per residue	13.8
Dihedral angle restraints	72
Mean dihedrals per residue	5.1
Total restraints	314
Total restraints per residue	22.4
Total number of atoms	455
Total dihedral angles	93
All-atom RMSD (Å)	0.68

<sup>a</sup> Each G:C base-pair in the stem was constrained by three hydrogen bonds.

shown). All 15 of the final structures (see below) have A695  $\gamma$  in the *trans* conformation.

### Structure calculations

Non-exchangeable inter-proton distances were obtained from 2D NOESY experiments with 60, 100 and 150 ms mixing times. The average buildup rate of the C689 H5/H6 and U697 H5/H6 NOEs was used to scale the NOE cross-peak intensities to determine distances (see Materials and Methods). A total of 193 NOE-derived distances and 72 dihedral-angle restraints (Table 1) were used for simulated annealing and refinement protocols as outlined in Materials and Methods. The three G-C base-pairs in the stem were restrained with nine Watson-Crick hydrogen bonds.

After simulated annealing, 60% of the random structures (24 out of 40) converged into global fold structures that formed the proper stem base-pairs and had an NOE penalty of less than 35 kcal/mol. Fifteen of these structures were randomly selected for refinement calculations (see Materials and Methods). None of the refined structures had more than two distance constraint violations greater than 0.2 Å. The root-mean-squared deviation (RMSD) from ideal angles for each of the 15 structures was less than  $2.8^\circ$ . The superposition of all 15 structures yielded an all-atom average RMSD of 0.68 Å (Table 1 and Figure 6).

## Discussion

### The structure of the 690 loop

Figure 7 shows a stereo view of the 690 hairpin tertiary structure. The 690 stem forms a hairpin with an A-type helical conformation and the loop forms a highly ordered structure that is stabilized by a network of hydrogen bonds (Table 2). The loop contains four structural motifs that contribute to loop stability and appear to be important for ribosome function: (i) a novel sheared G690·U697 mismatch, (ii) a sheared G691·A696 mismatch, (iii) a U-turn, and (iv) contiguous stacking of residues G693 to U697 (Figure 8). The structure of the 690 hairpin resembles a number of other biologi-

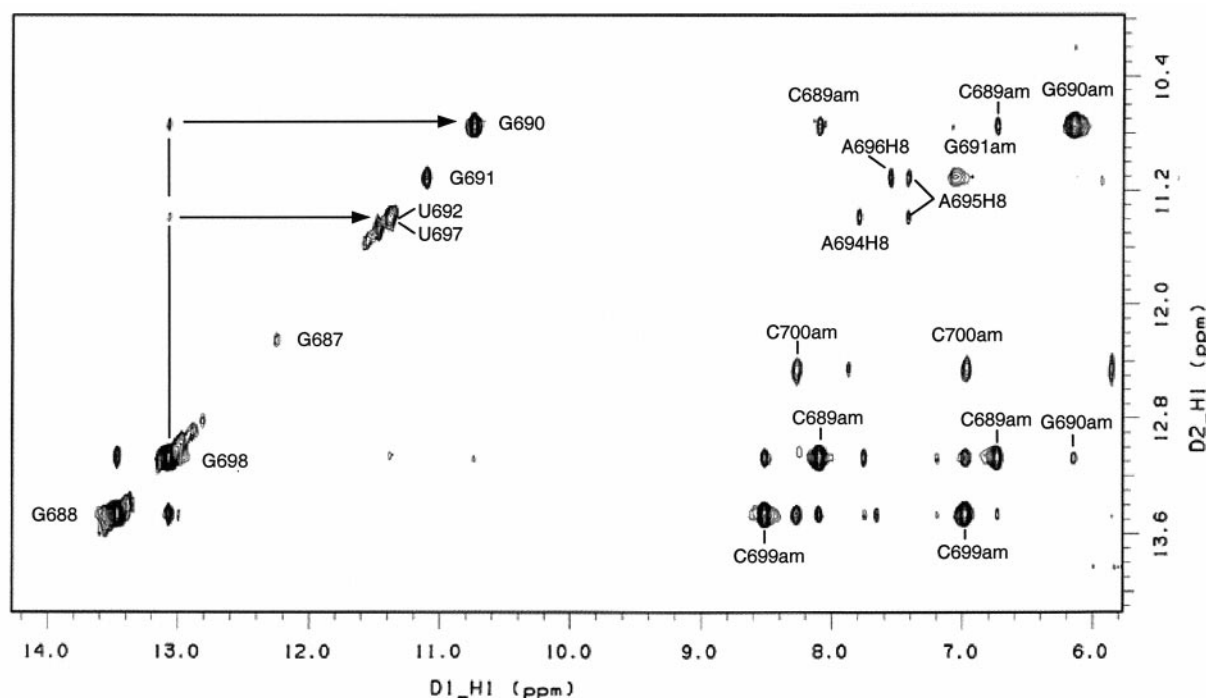


**Figure 5.** Imino/amino proton region of the 2D H<sub>2</sub>O NOESY collected at 200 ms mixing time and 5°C. Several key NOEs are observed from G691 and U692 imino protons to base protons of the adenine bases across the loop. Weak NOEs between the G698 imino proton from the stem to the G690 and U697 imino protons of the loop (shown by arrows) confirmed imino proton assignments. Note the absence of the NOE between G690 and U697 imino groups, indicating that G690 and U697 do not form a wobble pair and that these imino groups are > 4.0 Å apart.

cally important RNAs including the tRNA anticodon (Figure 9) and TΨC loops (Basavappa & Sigler, 1991; Quigley & Rich, 1976) and hexaloop hairpins (Fountain *et al.*, 1996; Huang *et al.*, 1996; Stallings & Moore, 1997). It is interesting, that each of these hairpins is known to participate in receptor interactions with proteins and RNA, suggesting that the 690 loop plays a similar role in the ribosome (see below).

### The G690·U697 mismatch

The G·U mismatch is the most frequent non-canonical base-pair in RNA. Over 1% of the paired positions in 16 S and 23 S rRNA are G·U mismatches (Gautheret *et al.*, 1995). Five different G·U mismatch structures have been reported (Nagaswamy *et al.*, 2000). Of these five, the G·U

wobble pair is by far the most common (He *et al.*, 1991). The other structures observed to date are G·U reverse wobble (Gautheret *et al.*, 1995; Nagaswamy *et al.*, 2000), G imino:amino-U-4 carbonyl bifurcated (Dallas & Moore, 1997), G·U carbonyl-imino (1 H-bond) (Jiang & Patel, 1998), and G·U imino-2-carbonyl (1 H-bond) (Allain & Varani, 1995). The structure of the 690 loop reveals a novel G690·U697 mismatch at the base of the loop (Figure 8). Based on modeling studies, a non-wobble structure for G690·U697 was previously suggested (Gautheret *et al.*, 1995), although the precise geometry was not predicted. Therefore, G·U mismatches may assume a variety of diverse structures depending on the context.

The G·U pair observed in the NMR structure of the 690 loop involves a single hydrogen bond from

**Table 2.** Hydrogen bond distances (Å) in the 690 loop

Donor	Acceptor	Average <sup>a</sup>	Range
G690 H22	U697 O4	1.90±0.22	1.80-2.17
A696 H62	G691 N3	3.05±0.64	2.50-3.58
G691 H22	A696 N7	2.04±0.13	1.91-2.29
G691 H21	A696 O1P	2.48±0.82	1.81-4.24
A695 H62	U691 O2'	2.89±0.63	2.10-4.27
U692 OH2'	A694 N7	1.77±0.07	1.69-1.95
U692 H3	A695 O1P	2.28±0.39	1.90-3.41

<sup>a</sup> Distance calculations are done for 15 final structures.



**Figure 6.** Superposition of the 15 final structures of the 690 loop. The all-atom RMSD is 0.68 Å. Water molecules and counterions included in the modeling are not shown for clarity.

G690-H22 (amino) to U697-O4 and belongs to the class of sheared mismatches (Leontis & Westhof, 1998). The average distance of this H-bond in the

15 final structures is 1.9 Å (Table 2), which is in the range for a direct H-bond. The G690·U697 pair is further stabilized by extensive stacking with the sheared G691·A696 pair. Figure 8(c) shows the 33.2 Å<sup>2</sup> van der Waals overlap of the two consecutive mismatches. The Watson-Crick functional groups of U697 are displaced toward the minor groove and are accessible to solvent. This suggests that broadening of the U697 imino proton resonance is due to solvent exchange (Figure 4). Furthermore, no NOE is observed between the G690 and U697 imino proton resonances (Figure 5) indicating that these protons are separated by a longer distance than in wobble or bifurcated G·U pairs. Since weak NOEs from G698-H1 to both G690-H1 and U697-H3 are observed, it seems unlikely that the absence of the G690 to U697 imino proton NOE is due to solvent exchange. Positioning of the U697 in the sheared orientation requires a larger helical twist (82° observed) than that which would be observed in an A-form conformation (32.7°) (Lavery & Sklenar, 1989). A weak NOE from U697-H5 to G698-H1' (data not shown) provides evidence for the unusual helical twist. Unrestrained molecular dynamics simulation with the AMBER 5.0 forcefield (Cornell *et al.*, 1995) with PME electrostatics (York *et al.*, 1993), explicit solvation, and counterions at 288 K showed that the G690-H22 amino to U697-O4 hydrogen bond was preserved throughout the 800 ps simulation.

In our mutational studies, the potential to form 690·697 sheared pairs correlates with ribosome function suggesting that the 690·697 sheared conformation is important for ribosome function (Morosyuk *et al.*, 2001). All nucleotide pairs except G:C and C:G can potentially form sheared confor-

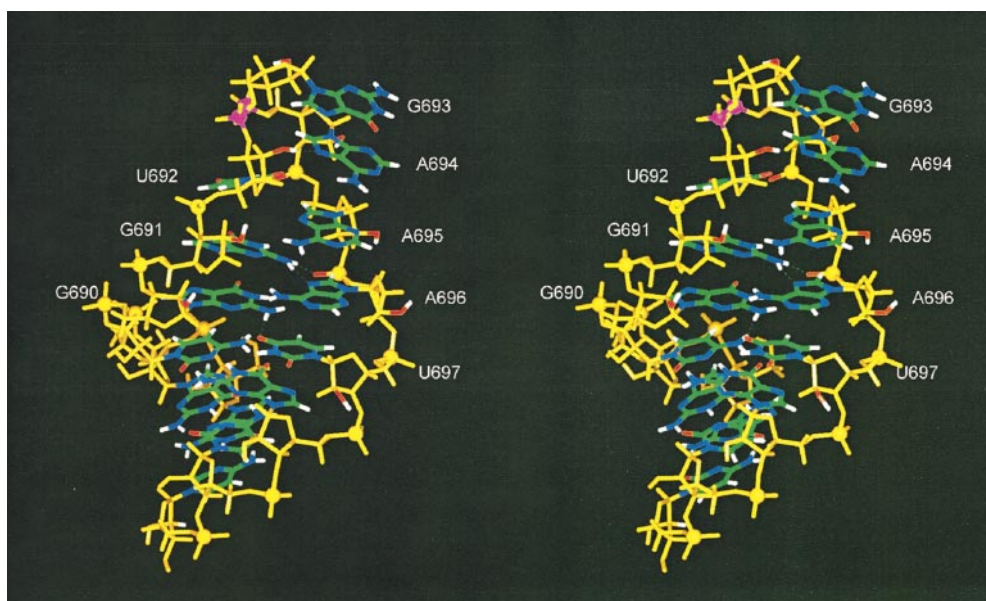


**Figure 7.** Stereo view of the 690 loop structure. The sugar-phosphate backbone is colored orange and base atoms are colored according to atom type to illustrate the locations of functional groups. The two phosphate groups with shifted <sup>31</sup>P resonances on the top of the loop are in purple. Loop nucleotides are labeled.

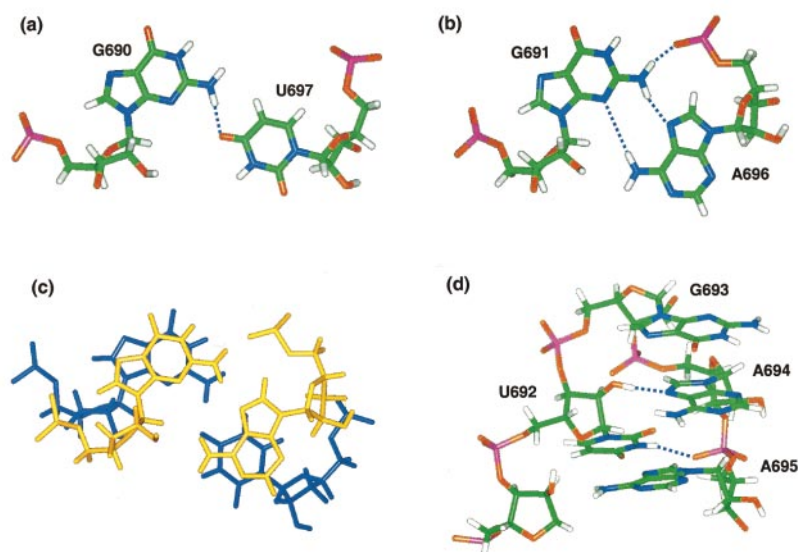


**Figure 8.** Details of the 690 loop structure. Hydrogen bonds are shown with broken lines (see Table 2 for listing of H-bond lengths). (a) Novel G690·U697 sheared base-pair with one H-bond between the G690 amino group and U697 O4. (b) The G691·A696 sheared pair. The H-bond between A696 H6 amino and G691 N3 is about 3 Å and is probably mediated by a water molecule. (c) Stacking interactions between the two mismatches at the base of the 690 loop. Extensive overlap (33.2 Å<sup>2</sup>) of aromatic rings is observed of the G690·U697 pair (blue) with the G691·A696 pair (orange). (d) The U-turn motif showing the three hydrogen bonds that stabilize the turn (see the text).

mations (see Figure 7 in Morosyuk *et al.*, 2001). In our mutational studies, the G:C and C:G mutants produced ribosomes with the lowest function of all 16 690:697 pairs. In addition, about 8% of phylogenetic rRNA sequences have a G690A substitution, creating the potential to form a Watson-Crick A690-U697 pair. Based on our mutagenesis and NMR results for the wild-type G·U sequence, we predict that the A690:U697 mutant is not Watson-Crick paired but forms a sheared type of geometry

without direct H-bonding and is stabilized by stacking with the sheared G691·A696 (see below) and interactions with other parts of the ribosome. Alternatively, the A690 mutant may participate in a dynamic exchange between Watson-Crick and sheared conformations.

It is interesting, that the NMR structure of loop IIa of yeast U2 snRNA (rGGUCAGUGUAACAACUGACC) is similar to the structure of the 690 hairpin with a U-turn, stacked purine bases on the

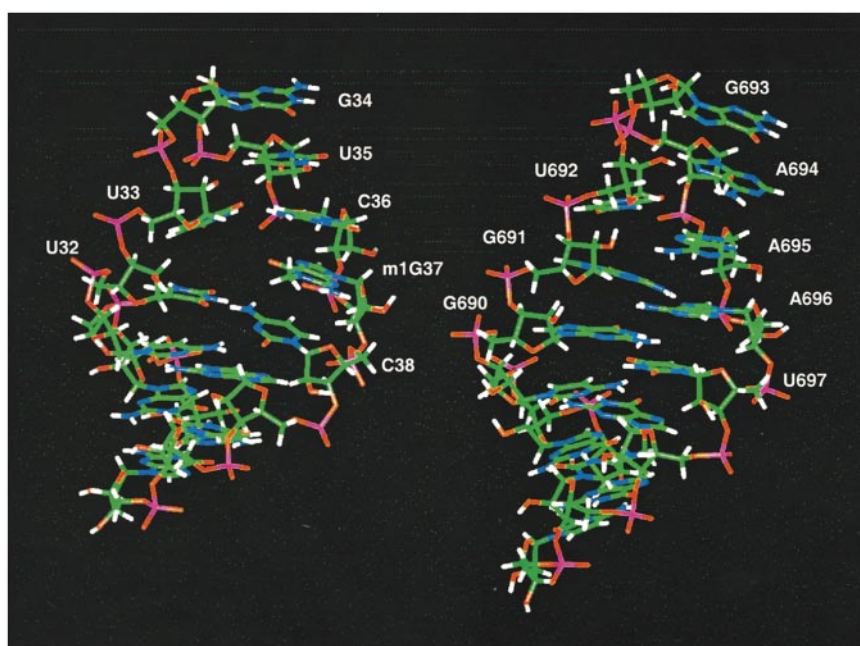


**Figure 9.** Comparison of the structures of the tRNA<sup>asp</sup> anticodon loop (Moras *et al.*, 1985) with the 690 loop of 16 S rRNA. Note the similar positions of the sheared U32·C38 pair, the U-turn, and the five stacked nucleotides on the 3'-side of the loop in tRNA and corresponding positions in the 690 loop. Also note that tRNA does not contain a residue analogous to G691.

3' side of the loop and a sheared G·A pair next to a closing non-standard U·A (Stallings & Moore, 1997). In that study, the loop closing U:A pair does not display a U-imino to A-H2 NOE, which is normally observed in a U-A Watson-Crick pair and the A is reactive to DMS probing (Ares & Igel, 1990). These data indicate that the closing U:A pair in loop IIa of U2 snRNA is not forming a Watson-Crick pair; instead, this U·A pair probably forms a sheared conformation (see the accompanying paper, Figure 7, Morosyuk *et al.*, 2001) or may be in dynamic conformational exchange.

### The G691·A696 sheared pair

The sheared G·A structure is a common motif and is frequently observed as the closing mismatch of hairpin loops (Heus & Pardi, 1991; Huang *et al.*, 1996; Jucker *et al.*, 1996; Pley *et al.*, 1994a; Stallings & Moore, 1997). It is also found in other contexts such as the sarcin-ricin loop (Szewczak & Moore, 1995), 5 S rRNA loop E (Correll *et al.*, 1997; Wimberly *et al.*, 1993), and tandem G·A pairs (Pley *et al.*, 1994b; SantaLucia & Turner, 1993). The G691·A696 mismatch of the 690 loop forms a sheared pair and is shown in Figure 8(b). The sheared G691·A696 structure is stabilized by stacking with the sheared G690·U697 pair (Figure 8(c)) and by H-bonds from G691-amino to A696-N7 and from G691-amino to the A696 non-bridging phosphate oxygen (Table 2); these H-bonds are also seen in GNRA tetraloops (Heus & Pardi, 1991) and tandem G·A pairs (SantaLucia & Turner, 1993). The G691·A696 pair, however, also shows differences in hydrogen bonding from previously observed sheared G·A pairs. Unlike GNRA tetraloops and tandem G·A structures, the distance between A696-N6H and G691-N3 is about 3 Å, which is too long to form a direct hydrogen bond but may instead be mediated by a water molecule. This is similar to the crystal structure of the GAAA loop complex with its receptor, which also does not show a direct A-N6H to G-N3 H-bond (Pley *et al.*, 1994a). In addition, no H-bond is observed from A696-N6H to G691-O2', which is observed in the tandem G·A structure (SantaLucia & Turner, 1993). In the instant-evolution experiment, the only functional substitutions isolated for the wild-type G691·A696 were A·A, U·A, and G·G (Morosyuk *et al.*, 2001). All three of these substitutions have previously been shown to be capable of forming sheared structures that are isomorphous with G691·A696 (see Morosyuk *et al.*, 2001). This suggests that the sheared G691·A696 conformation observed is important for ribosome function.

### The U-turn

The change in direction of the phosphate backbone in the 690 loop is governed by a U-turn structure (Figure 8(d)), a common motif found in tRNA anticodon (Figure 9) and TΨC loops (Basavappa & Sigler, 1991; Quigley & Rich, 1976), hexaloop hair-

pins (Huang *et al.*, 1996), tetraloop hairpins (Jucker *et al.*, 1996), and a pseudoknot structure (Gutell *et al.*, 2000; Kolk *et al.*, 1998). The structure of the classical U-turn with UNR sequence is typically stabilized by two H-bonds: one from the U-OH2' to the N7 of the  $n + 2$  purine and the second from the U imino proton to the bridging or non-bridging oxygen of the  $n + 3$  phosphate. The U692-G693-A694 U-turn in the 690 loop is consistent with this description. The 690 loop has H-bonds from U692-OH2' to A694-N7 and from U692-imino to A695-O1P (non-bridging) (Table 2). The 17 Hz linewidth of the U692 imino proton resonance is comparable with the H-bonded stem imino protons, which is also consistent with H-bonding for the U692 imino proton.

The backbone turn in the 690 loop is accomplished in part by the *trans* G693  $\alpha$  torsion angle that produces a downfield shift of the G693 <sup>31</sup>P resonance (-2.69 ppm) (Figure 3). The A694 <sup>31</sup>P is also slightly downfield shifted (-3.08 ppm) (Figure 3). The A694 dihedral angles, however, are within the A-form range. The dihedral angle for the A695  $\alpha$  is -137°, which is slightly outside the range typically observed for a non-shifted <sup>31</sup>P resonance (-3.81 ppm). Corresponding shifted <sup>31</sup>P resonances and dihedral angles were observed in the loop IIa of U2 snRNA (Stallings & Moore, 1997) and also in the L11 protein hexaloop of 23 S rRNA (Fountain *et al.*, 1996).

Phylogenetic data suggest that the U-turn motif in the 690 loop may be functionally important. U692 is conserved in 99.6% of bacterial sequences and position 694 is always a purine (A in 87.6% or G in 12.4% of rRNA sequences) (Gutell *et al.*, 2000; Van de Peer *et al.*, 1999). All of the 690 loop instant-evolution mutants are able to form a turn at the top of the hairpin, although 55 functional sequences were isolated that do not adhere to the UNR U-turn motif (Morosyuk *et al.*, 2001). These data suggest that a turn in the loop is important but that it does not have to be a U-turn to maintain ribosome function. Two consequences of the U-turn in the 690 loop appear to be important for ribosome function. First, the U-turn places G693 at the top of the loop. A number of studies have implicated this residue in ribosome function (Doring *et al.*, 1994; Moazed & Noller, 1986, 1990) and recent crystal structures of the 30 S subunit show G693 stacked on N1 of the E site codon of an mRNA mimic (Wimberly *et al.*, 2000).

The second consequence of the U-turn in the 690 loop is the contiguous stacking of residues G693 to U697, which appear to be involved in ribosomal subunit association (see below) (Cate *et al.*, 1999). Nucleotides G693 to U697 form an uninterrupted array of stacked bases on the 3' side of the stem. The parallel stacking of these bases place the adenine ( $n$ ) H2 protons of A694, A695, and A696 within 3 Å of the ( $n + 1$ ) H1' protons. These findings are supported by the 2D NOESY data (Figure 2). The Watson-Crick functional groups of residues G693 to U697 are displaced toward the

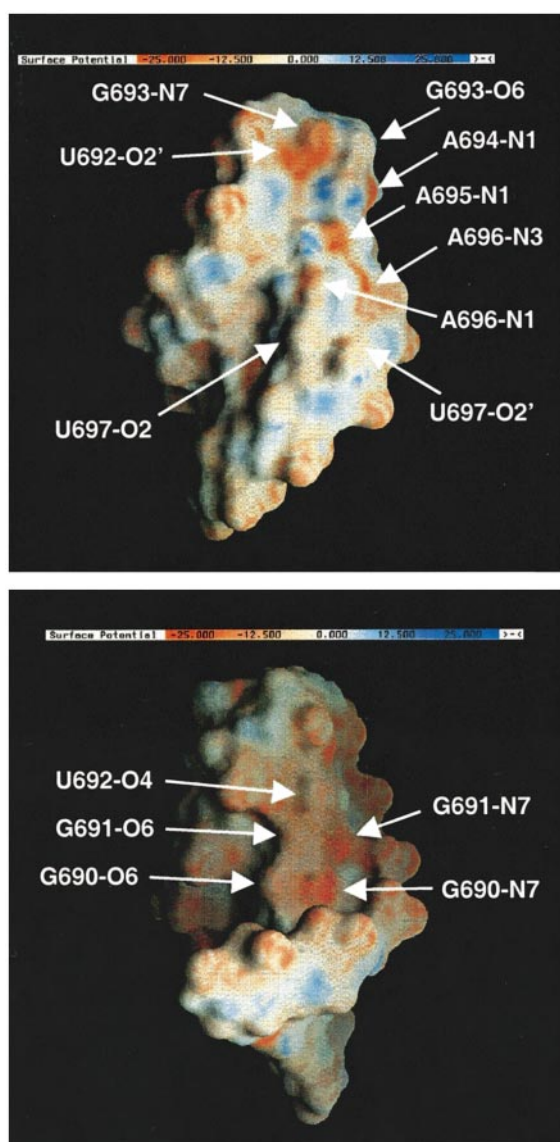


**Figure 10.** Surface potential of the 690 loop with views into the minor groove (top) and major groove (bottom). The surface potential was calculated using QNIFFT, using a two step focusing procedure as described previously (Chin *et al.*, 1999) and displayed with GRASP. The simulated salt concentration was 145 mM and the dielectric was assumed to be 80 for water and 2 for the RNA. The most prominent electrostatic features are labeled. These electronegative groups (red surfaces) may be important for ligand recognition and/or metal binding.

minor groove of the loop while the Hoogsteen edges of these bases interact with the opposite strand. The six-membered ring of A694 is positioned directly above the H1' of A695; this apparently causes an upfield shift of the A695-H1' resonance (Figure 2). Similar upfield shifts of H1' resonances due to aromatic stacking have been observed in the GAGA and UUCG tetraloop (Jucker *et al.*, 1996; Varani *et al.*, 1991) as well as

tandem G·A mismatch structures (SantaLucia & Turner, 1993).

### Interactions with other ligands

The 690 loop, stem and adjacent internal loop have been implicated in RNA-RNA interactions with the large subunit (Cate *et al.*, 1999; Merryman *et al.*, 1999b). Given the similarity between the GAAA tetraloop and the 690 loop structures (the U turn, sheared G·A motifs and 3'-base stacking), it is possible that the 690 loop interacts with another helical region of the 23 S rRNA with a mechanism similar to that described for the GAAA tetraloop receptor (Pley *et al.*, 1994a). In the GAAA-receptor model, N1, N3, and 2'-OH groups of the adenine bases interact with the minor groove of consecutive G-C pairs in the receptor stem. The 690 region has been shown to form a bridge (B7) between the small and large ribosomal subunits (Cate *et al.*, 1999). The edge of the cleft in the 50 S subunit interface (Ban *et al.*, 1999), where the counterpart of the 690 loop bridge B7 maps (Cate *et al.*, 1999), appears to consist of domain IV of 23 S rRNA (Mueller *et al.*, 2000). In domain IV, the 1700 and 1920 regions are protected from hydroxyl radical cleavage upon subunit association (Merryman *et al.*, 1999a). The 1920 region in 23 S rRNA and the 790 loop in 16 S rRNA must be close in 70 S ribosomes because they both are cleaved by hydroxyl radicals generated from the 5' end of the same P-site bound tRNA anticodon stem-loop (Joseph *et al.*, 1997). The 790 and 690 loops have been crosslinked (Atmadja *et al.*, 1986) and found in close proximity in the platform region of the 30 S structure (Clemons *et al.*, 1999). This places the 690 loop in the vicinity of domain IV of 23 S ribosomal RNA.

In the 690 loop, S11 produces weak protection from hydroxyl radicals (Powers & Noller, 1995) and strong protection from base-specific probes (Stern *et al.*, 1988) (Figure 1(a)). This suggests that the S11 protein may interact with the minor groove functional groups of the 690 loop as well as the adjacent internal loop. The 690 region and the adjacent internal loop probably undergo structural rearrangements and may interact with these ligands at different stages of protein synthesis (Agrawal *et al.*, 1998; Joseph *et al.*, 1997; McCutcheon *et al.*, 1999; Moazed & Noller, 1989; Mueller *et al.*, 1997; Stark *et al.*, 1997). This hypothesis provides an explanation for how the same nucleotides in the 690 region can have footprints and crosslinks to P-site tRNA, S11, and the 50 S subunit. Insight into the nature of the proposed interactions of the 690 loop with its ligands is provided by electrostatic surface of the 690 loop shown in Figure 10 (Chin *et al.*, 1999). In the major groove, the carbonyl oxygen atoms of G690, G691, and U692 are aligned and form a string of electronegative groups. In the minor groove, the O2 of U697 is a prominent feature as are the string of phosphate, O2', and adenine N3 groups. These electronegative surfaces may be important for

ligand recognition of the large subunit, S11, and/or metal binding.

### Comparison of the solution and crystal structures of the 690 loop

While this paper was under review, two independent crystal structures of the 30 S subunit were published (Schluenzen *et al.*, 2000; Wimberly *et al.*, 2000). The heavy-atom RMSD for residues 688 to 699 of 16 S rRNA between the NMR structure and the Schluenzen *et al.* (2000) structure is 1.77 Å and with the Wimberly *et al.* (2000) structure is 0.79 Å, respectively. The Wimberly *et al.* (2000) structure is in quantitative agreement with the NMR structure and contains all of the features revealed in the NMR structure including the sheared G690·U697 mismatch. The Schluenzen *et al.* (2000) structure has the same overall fold as the NMR structure and contains a U-turn closed by a sheared G691·A696 mismatch, but does not show the sheared G690·U697 mismatch and does not have the contiguous stacking of residues G693 to U697. The differences between the Schluenzen *et al.* structure and the NMR and the Wimberly *et al.* structures may reflect a different functional state of the 690 loop or may be due to slightly lower resolution (3.3 *versus* 3.05 Å) and incomplete refinement as stated by the authors (Schluenzen *et al.*, 2000). The agreement between the Wimberly *et al.* structure and the NMR structure is remarkable, since the X-ray structure reveals that the 690 loop forms up to 11 hydrogen bonds with the 790 loop, five H-bonds to the S11 protein, and shows stacking of G693 with the N1 base of the E-site codon mimic, while the NMR structure is not complexed with any other molecule. This suggests that the 690 loop is properly folded prior to the binding of S11 and may assist in the folding and assembly of the ribosome, including the 790 loop for which the NMR structure is more dynamic (S. Varma, P.R.C. and J.S., unpublished results). Functional aspects of interactions of the 690 loop with other ribosomal components are discussed in the accompanying paper (Morosyuk *et al.*, 2001).

## Materials and Methods

### RNA sample preparation

The unlabeled 14mer RNA oligoribonucleotide was synthesized on solid support with the phosphoramidite method (Capaldi & Reese, 1994) on a Cruachem PS 250 DNA/RNA synthesizer. Oligomers were removed from the solid support and deprotected by treatment with ammonia and acid following the manufacturer's protocol and purified by denaturing gel electrophoresis, as described previously (Morosyuk *et al.*, 2000). UV absorbance melting of the 14mer indicated a concentration-independent  $T_M$  over an 80-fold range of concentration ( $T_M = 57.9^\circ\text{C}$  in 40 mM NaCl, 10 mM sodium cacodylate, 0.1 mM EDTA, (pH 6) buffer; complete results for the wild-type and mutants will be reported elsewhere), confirming the formation of the expected unimolecular

hairpin under the NMR solution conditions (Morosyuk *et al.*, 2000).

The uniformly labeled sequence was transcribed *in vitro* using uniformly  $^{13}\text{C}$ ,  $^{15}\text{N}$ -labeled NTPs. Uniformly  $^{13}\text{C}$ ,  $^{15}\text{N}$ -labeled NTPs were synthesized according to published procedures (Batey *et al.*, 1992; Nikonowicz *et al.*, 1992). Phage T7 RNA polymerase and uniformly  $^{13}\text{C}$ ,  $^{15}\text{N}$  labeled NTPs were used to synthesize the 14mer RNA by run-off transcription (Wyatt *et al.*, 1991). The 14mer RNA was purified by denaturing urea 20% (w/v) polyacrylamide gel electrophoresis, excising the appropriate gel band, and extracting by the crush and soak method. Extracted samples were extensively dialyzed against double-distilled, deionized water, lyophilized, and dissolved in NMR buffer. The NMR buffer consisted of 50 mM NaCl, 0.2 mM EDTA, 10 mM disodium phosphate at pH 6.8 and was prepared in either 90%  $\text{H}_2\text{O}$  and 10%  $^2\text{H}_2\text{O}$  or 99.9%  $^2\text{H}_2\text{O}$  for use in exchangeable or non-exchangeable proton spectroscopy, respectively. The samples for non-exchangeable proton NMR studies were lyophilized several times from 99.96%  $^2\text{H}_2\text{O}$  and finally dissolved in 99.996%  $^2\text{H}_2\text{O}$ . Each NMR sample contained 3-trimethylsilyl propionic-2,2,3,3- $\text{d}^4$  (TSP) for referencing the spectra to a proton frequency of 0.0 ppm. Trimethyl phosphate (TMP) was used as an external standard for  $^{31}\text{P}$  referencing at 0.0 ppm.

### NMR methods

All NMR spectra were recorded on a Varian UNITY 500 MHz NMR spectrometer equipped with a  $^1\text{H}$ ,  $^{13}\text{C}$ ,  $^{15}\text{N}$ ,  $^{31}\text{P}$ -quadruple resonance probe with z-axis gradient coil (Nalorac, Inc.). The carrier frequency was set at the  $\text{H}^2\text{HO}$  resonance for proton,  $-3.5$  ppm for  $^{31}\text{P}$ , and 148 or 78 ppm for  $^{13}\text{C}$ . After acquisition, data were transferred to a Silicon Graphics (Indigo<sup>2</sup> Extreme) workstation and processed with VNMR or FELIX 98 (MSI) software.

Exchangeable proton 1D and 2D spectra were acquired at  $1^\circ\text{C}$  or  $5^\circ\text{C}$  using WATERGATE with "flip-back" solvent suppression (Lippens *et al.*, 1995; Piatto *et al.*, 1992) as described by Morosyuk *et al.* (2000). 2D NOESY spectra for non-exchangeable protons were collected at  $15^\circ\text{C}$  using mixing times of 60 ms, 100 ms, 150 ms and 500 ms mixing times. 2D NOESY at 500 ms mixing time were collected at two temperatures,  $15^\circ\text{C}$  and  $20^\circ\text{C}$ , that facilitated peak assignments due to slight changes in chemical shift for some resonances. The residual  $\text{H}^2\text{HO}$  peak was irradiated for one second with low power during recycle delay in order to reduce the intensity of the  $\text{H}^2\text{HO}$  peak to about the same magnitude as the RNA peaks. Quadrature detection for the indirect dimensions of multidimensional experiments was achieved using the States-TPPI method (Marion *et al.*, 1989). Acquisition times for 2D experiments were 24 to 36 hours. The data were zero filled in the  $t_1$  dimension and processed with appropriate skewed-sinebell apodization functions.

All other multidimensional experiments were recorded at  $15^\circ\text{C}$  in 99.996%  $^2\text{H}_2\text{O}$ . 2D spectra included  $^{31}\text{P}$  decoupled DQF-COSY (Varani & Tinoco, 1991),  $^{31}\text{P}$ - $^1\text{H}$  HETCOR (Sklenar *et al.*, 1986), and 2D HcCH-TOCSY optimized for AH2-AH8 correlation (Marino *et al.*, 1994). Dihedral angle restraints were derived from  $J$ -coupling measurements of  $^{31}\text{P}$ -decoupled DQF-COSY and  $^{31}\text{P}$ - $^1\text{H}$  HETCOR cross-peaks (Varani & Tinoco, 1991).

Three-dimensional heteronuclear NMR experiments that were performed using the uniformly  $^{13}\text{C}$ ,  $^{15}\text{N}$  labeled sample included 3D HMQC-NOESY at 200 ms mixing time with the carbon carrier frequency set in the C8/C6 region of the spectrum at 135 ppm (Fesik & Zuiderweg, 1990), 3D HCcH TOCSY, 3D hCCH TOCSY, and 3D HCcH COSY (Hall, 1995; Nikonowicz & Pardi, 1992, 1993; Pardi, 1995; Varani *et al.*, 1996) and 3D HCcH E-COSY (Schwalbe *et al.*, 1994). The FIDs were zero filled to give a final matrix of  $128 \times 128 \times 2048$  real points. A combination of these experiments was used for peak assignments and to generate the distance restraints.

### Structure calculations

Structures were calculated with X-PLOR version 3.1 using restrained molecular dynamics (rMD) and restrained energy minimization (rEM) (Brünger, 1992), and structures were analyzed using Biosym Insight II (MSI). Non-exchangeable inter-proton distances were obtained from 2D NOESY experiments with 60, 100 and 150 ms mixing times. Cross-peak volumes were integrated using the FELIX (MSI) software package. The average buildup rates of C689 H5/H6 and U697 H5/H6 NOEs were used to scale other NOE buildup rates. Error bars were assigned to each distance as follows: 2.0-2.6 ( $\pm 0.4$ ) Å, 2.7-3.3 ( $\pm 0.5$ ) Å, 3.4-4.0 ( $\pm 0.7$ ) Å, 4.0-5.0 ( $\pm 0.9$ ) Å (SantaLucia & Turner, 1993). Error ranges were set to larger values in some instances to account for spectral overlap and spin diffusion. A few weak cross-peaks only observed at 500 ms mixing time NOESY were restrained to 3.0-6.0 Å distance. The 24 distance constraints involving exchangeable protons were obtained from 2D H<sub>2</sub>O NOESY experiment at 200 ms mixing time and were classified as strong (1.5-3.0 Å), medium (2.5-4.5 Å), or weak (3.0-6.0 Å) distance restraints.

NOE and dihedral angle restraints were included in the force field as a quadratic pseudopotential with a flat well within the upper and lower bounds of the restraints. Force constants used for the NOE and dihedral angle potentials were set to 50 kcal/(mol Å<sup>2</sup>) and 50 kcal/(mol rad<sup>2</sup>). Calculations were performed in four stages. First, 40 structures with random dihedral angles were generated using the X-PLOR internal coordinate facility and used as the starting coordinates for the rMD and rEM protocols. Second, during the global fold phase, a simulated annealing protocol *in vacuo* was used in which only NOE and hydrogen bonding distance constraints were used together with energy terms to maintain the covalent structure. Repulsive van der Waals' interactions were turned off initially to facilitate sampling of conformational space and improve convergence (SantaLucia & Turner, 1993). The *in vacuo* global fold calculation without dihedral restraints and the initial *in vacuo* refinement with dihedral restraints were performed as described previously (SantaLucia & Turner, 1993). Several trial global fold calculations were performed to examine structures for inter-proton distance violations. Eighteen "missing NOE" distance restraints ( $>4$  Å) were added to the restraint file to increase distances between protons which did not produce NOE cross-peaks in the NMR spectra but were close in the global fold structures (Stallings & Moore, 1997). Incorporation of the "missing NOE" restraints improved the convergence of the global fold structures. A convergence rate of 60% of the random structures (24 out of 40) was observed. Next, the global fold structures were refined following the protocol described previously using the

complete set of NOE and dihedral restraints (SantaLucia & Turner, 1993). A control set of calculations were performed without imposing the  $\alpha$  and  $\zeta$  dihedral restraints derived from  $^{31}\text{P}$  chemical shifts; these *in vacuo* refined structures (not shown) were within the RMSD of the structures calculated with the  $\alpha$  and  $\zeta$  restraints included. Final structures were evaluated on the basis of total NOE restraint violation energy. At the final refinement stage, the structures were subjected to rMD and energy minimization using Amber version 5 (Oxford Molecular, Inc.) utilizing particle mesh Ewald (PME) electrostatics and including the explicit TIP3P solvent and 13 solvated sodium ions to neutralize phosphate backbone charge of the 14mer RNA (Cornell *et al.*, 1995). The dynamics run included 50 ps of rMD at 288 K followed by 3000 steps of energy minimization. To validate the final structure, unrestrained 800 ps MD simulation with PME electrostatics, explicit solvation, and counterions at 288 K was performed on one randomly selected final structure. The all-atom RMSD of the structure after 800 ps of dynamics and the starting structure was 1.4 Å, indicating that the 690 loop forms a stable fold.

### Protein Data Bank accession codes

Coordinates have been deposited in the Protein Data Bank (accession code 1FHK).

### Acknowledgments

We thank Dr A. Pardi and Dr J. Puglisi for providing some of the 3D NMR pulse sequences used in this study and Dr N. Leontis, Dr A. Gulaev, and Dr Tom Cheatham for help with molecular modeling. We thank Michael J. Grey for performing the QNIFFT calculations and Dr Stephen R. Holbrook for performing stacking calculations. We thank Robin Gutell for useful discussions on the phylogeny of the 690 loop. This work was supported by NIH grants GM55745 and GM52896.

### References

- Agalarov, S. C. & Williamson, J. R. (2000). A hierarchy of RNA subdomains in assembly of the central domain of the 30 S ribosomal subunit. *RNA*, **6**, 402-408.
- Agalarov, S. C., Prasad, G. S., Funke, P. M., Stout, C. D. & Williamson, J. R. (2000). Structure of the S15, S6, S18-rRNA complex: assembly of the 30 S ribosome central domain. *Science*, **288**, 107-112.
- Agrawal, R. K., Penczek, P., Grassucci, R. A. & Frank, J. (1998). Visualization of elongation factor G on the *Escherichia coli* 70 S ribosome: the mechanism of translocation. *Proc. Natl Acad. Sci. USA*, **95**, 6134-6138.
- Allain, F. H. & Varani, G. (1995). Structure of the P1 helix from group I self-splicing introns. *J. Mol. Biol.* **250**, 333-353.
- Altona, C. (1982). Conformational analysis of nucleic acids. Determination of backbone geometry of single-helical RNA and DNA in aqueous solution. *Recueil. J. Roy. Netherlands Chem. Soc.* **101**, 413-433.
- Ares, M., Jr & Igel, A. H. (1990). Lethal and temperature-sensitive mutations and their suppressors identify an essential structural element in U2 small nuclear RNA. *Genes Dev.* **4**, 2132-2145.

- Atmadja, J., Stiege, W., Zobawa, M., Greuer, B., Osswald, M. & Brimacombe, R. (1986). The tertiary folding of *Escherichia coli* 16 S RNA, as studied by *in situ* intra-RNA cross-linking of 30 S ribosomal subunits with bis-(2-chloroethyl)-methylamine. *Nucl. Acids Res.* **14**, 659-673.
- Ban, N., Nissen, P., Hansen, J., Capel, M., Moore, P. B. & Steitz, T. A. (1999). Placement of protein and RNA structures into a 5 Å-resolution map of the 50 S ribosomal subunit. *Nature*, **400**, 841-847.
- Ban, N., Nissen, P., Hansen, J., Moore, P. B. & Steitz, T. A. (2000). The complete atomic structure of the large ribosomal subunit at 2.4 Å resolution. *Science*, **289**, 905-920.
- Basavappa, R. & Sigler, P. B. (1991). The 3 Å crystal structure of yeast initiator tRNA: functional implications in initiator/elongator discrimination. *EMBO J.* **10**, 3105-3111.
- Batey, R. T., Inada, M., Kujawinski, E., Puglisi, J. D. & Williamson, J. R. (1992). Preparation of isotopically labeled ribonucleotides for multidimensional NMR spectroscopy of RNA. *Nucl. Acids Res.* **20**, 4515-4523.
- Battiste, J. L., Pestova, T. V., Hellen, C. U. & Wagner, G. (2000). The eIF1A solution structure reveals a large RNA-binding surface important for scanning function. *Mol. Cell*, **5**, 109-119.
- Berglund, H., Rak, A., Serganov, A., Garber, M. & Hard, T. (1997). Solution structure of the ribosomal RNA binding protein S15 from *Thermus thermophilus*. *Nature Struct. Biol.* **4**, 20-23.
- Brünger, A. T. (1992). *X-PLOR 3.1: A System for Crystallography and NMR*, Yale University Press, New Haven, CT.
- Capaldi, D. C. & Reese, C. B. (1994). Use of the 1-(2-fluorophenyl)-4-methoxypiperidin-4-yl (Fmp) and related protecting groups in oligoribonucleotide synthesis: stability of internucleotide linkages to aqueous acid. *Nucl. Acids Res.* **22**, 2209-2216.
- Cate, J. H., Yusupov, M. M., Yusupova, G. Z., Earnest, T. N. & Noller, H. F. (1999). X-ray crystal structures of 70 S ribosome functional complexes. *Science*, **285**, 2095-2104.
- Chin, K., Sharp, K. A., Honig, B. & Pyle, A. M. (1999). Calculating the electrostatic properties of RNA provides new insights into molecular interactions and function. *Nature Struct. Biol.* **6**, 1055-1061.
- Clemons, W. M., Jr, May, J. L., Wimberly, B. T., McCutcheon, J. P., Capel, M. S. & Ramakrishnan, V. (1999). Structure of a bacterial 30 S ribosomal subunit at 5.5 Å resolution. *Nature*, **400**, 833-840.
- Cornell, W. D., Cieplak, P., Bayly, C. I., Gould, I. R. & Merz, K. M. *et al.* (1995). A 2nd generation force-field for the simulation of proteins, nucleic-acids, and organic molecules. *J. Am. Chem. Soc.* **117**, 5179-5197.
- Correll, C. C., Freeborn, B., Moore, P. B. & Steitz, T. A. (1997). Metals, motifs, and recognition in the crystal structure of a 5 S rRNA domain. *Cell*, **91**, 705-712.
- Dallas, A. & Moore, P. B. (1997). The solution structure of the loop E/loop D region of *E. coli* 5 S rRNA. *Structure*, **5**, 1639-1653.
- Doring, T., Mitchell, P., Osswald, M., Bochkariov, D. & Brimacombe, R. (1994). The decoding region of 16 S RNA: a cross-linking study of the ribosomal A, P and E sites using tRNA derivatized at position 32 in the anticodon loop. *EMBO J.* **13**, 2677-2685.
- Egebjerg, J. & Garrett, R. A. (1991). Binding sites of the antibiotics pactamycin and celesticetin on ribosomal RNAs. *Biochimie*, **73**, 1145-1149.
- Fesik, S. W. & Zuiderweg, E. R. (1990). Heteronuclear three-dimensional NMR spectroscopy of isotopically labelled biological macromolecules. *Quart. Rev. Biophys.* **23**, 97-131.
- Fountain, M. A., Serra, M. J., Krugh, T. R. & Turner, D. H. (1996). Structural features of a six-nucleotide RNA hairpin loop found in ribosomal RNA. *Biochemistry*, **35**, 6539-6548.
- Fourmy, D., Yoshizawa, S. & Puglisi, J. D. (1998). Paromomycin binding induces a local conformational change in the A-site of 16 S rRNA. *J. Mol. Biol.* **277**, 333-345.
- Frank, J. & Agrawal, R. K. (2000). A ratchet-like inter-subunit reorganization of the ribosome during translocation. *Nature*, **406**, 318-322.
- Gautheret, D., Konings, D. & Gutell, R. R. (1995). G:U base-pairing motifs in ribosomal RNA. *RNA*, **1**, 807-814.
- Gorenstein, D. (1984). Principles and applications. In *Phosphorus-31 NMR* (Gorenstein, D., ed.), pp. 7-36, Academic Press, Orlando, FL.
- Gutell, R. R., Cannone, J. J., Konings, D. & Gautheret, D. (2000). Predicting U-turns in ribosomal RNA with comparative sequence analysis. *J. Mol. Biol.* **300**, 791-803.
- Hall, K. B. (1995). Uses of <sup>13</sup>C and <sup>15</sup>N-labeled RNA in NMR of RNA-protein complexes. *Methods Enzymol.* **261**, 542-559.
- Hard, T., Rak, A., Allard, P., Kloo, L. & Garber, M. (2000). The solution structure of ribosomal protein L36 from *Thermus thermophilus* reveals a zinc-ribbon like fold. *J. Mol. Biol.* **296**, 169-180.
- He, L., Kierzek, R., SantaLucia, J., Jr, Walter, A. E. & Turner, D. H. (1991). Nearest neighbor parameters for GU mismatches: GU/UG is destabilizing in the contexts CGUG, UGUA, and AGUU but stabilizing in GGUC. *Biochemistry*, **30**, 11124-11132.
- Heus, H. A. & Pardi, A. (1991). Structural features that give rise to the unusual stability of RNA hairpins containing GNRA loops. *Science*, **253**, 191-194.
- Huang, S., Wang, Y. X. & Draper, D. E. (1996). Structure of a hexanucleotide RNA hairpin loop conserved in ribosomal RNAs. *J. Mol. Biol.* **258**, 308-321.
- Jaishree, T. N., Ramakrishnan, V. & White, S. W. (1996). Solution structure of prokaryotic ribosomal protein S17 by high-resolution NMR spectroscopy. *Biochemistry*, **35**, 2845-2853.
- Jiang, L. & Patel, D. J. (1998). Solution structure of the tobramycin-RNA aptamer complex. *Nature Struct. Biol.* **5**, 769-774.
- Joseph, S. & Noller, H. F. (1996). Mapping the rRNA neighborhood of the acceptor end of tRNA in the ribosome. *EMBO J.* **15**, 910-916.
- Joseph, S., Weiser, B. & Noller, H. F. (1997). Mapping the inside of the ribosome with an RNA helical ruler. *Science*, **278**, 1093-1098.
- Jucker, F. M., Heus, H. A., Yip, P. F., Moors, E. H. & Pardi, A. (1996). A network of heterogeneous hydrogen bonds in GNRA tetraloops. *J. Mol. Biol.* **264**, 968-980.
- Kolk, M. H., van der Graaf, M., Wijmenga, S. S., Pleij, C. W., Heus, H. A. & Hilbers, C. W. (1998). NMR structure of a classical pseudoknot: interplay of single- and double-stranded RNA. *Science*, **280**, 434-438.

- Lankhorst, P. P., Haasnoot, C. A., Erkelens, C. & Altona, C. (1984). Carbon-13 NMR in conformational analysis of nucleic acid fragments. 3. The magnitude of torsional angle epsilon in d(TpA) from CCOP and HCOP NMR coupling constants. *Nucl. Acids Res.* **12**, 5419-5428.
- Lavery, R. & Sklenar, H. (1989). Defining the structure of irregular nucleic acids: conventions and principles. *J. Biomol. Struct. Dynam.* **6**, 655-667.
- Leontis, N. B. & Westhof, E. (1998). Conserved geometrical base-pairing patterns in RNA. *Quart. Rev. Biophys.* **31**, 399-455.
- Lippens, G., Dhalluin, C. & Wieruszkeski, J. M. (1995). Use of a water flip-back pulse in the homonuclear NOESY experiment. *J. Biomol. NMR*, **5**, 327-331.
- Mankin, A. S. (1997). Pactamycin resistance mutations in functional sites of 16 S rRNA. *J. Mol. Biol.* **274**, 8-15.
- Marino, J. P., Prestegard, J. H. & Crothers, D. M. (1994). Correlation of adenine H2/H8 resonances in uniformly <sup>13</sup>C-labeled RNAs by HCCH-TOCSY: a new tool for <sup>1</sup>H assignment. *J. Am. Chem. Soc.* **116**, 2205-2206.
- Marion, D., Ikura, M., Tschudin, R. & Bax, A. (1989). Rapid recording of 2D NMR-spectra without phase cycling: application to the study of hydrogen-exchange in proteins. *J. Magn. Reson.* **85**, 393-399.
- Markus, M. A., Gerstner, R. B., Draper, D. E. & Torchia, D. A. (1998). The solution structure of ribosomal protein S4 delta41 reveals two subdomains and a positively charged surface that may interact with RNA. *EMBO J.* **17**, 4559-4571.
- McCutcheon, J. P., Agrawal, R. K., Philips, S. M., Grassucci, R. A., Gerchman, S. E. & Clemons, W. M., Jr *et al.* (1999). Location of translational initiation factor IF3 on the small ribosomal subunit. *Proc. Natl Acad. Sci. USA*, **96**, 4301-4306.
- Merryman, C., Moazed, D., Daubresse, G. & Noller, H. F. (1999a). Nucleotides in 23 S rRNA protected by the association of 30 S and 50 S ribosomal subunits. *J. Mol. Biol.* **285**, 107-113.
- Merryman, C., Moazed, D., McWhirter, J. & Noller, H. F. (1999b). Nucleotides in 16 S rRNA protected by the association of 30 S and 50 S ribosomal subunits. *J. Mol. Biol.* **285**, 97-105.
- Moazed, D. & Noller, H. F. (1986). Transfer RNA shields specific nucleotides in 16 S ribosomal RNA from attack by chemical probes. *Cell*, **47**, 985-994.
- Moazed, D. & Noller, H. F. (1989). Intermediate states in the movement of transfer RNA in the ribosome. *Nature*, **342**, 142-148.
- Moazed, D. & Noller, H. F. (1990). Binding of tRNA to the ribosomal A and P sites protects two distinct sets of nucleotides in 16 S rRNA. *J. Mol. Biol.* **211**, 135-145.
- Moazed, D., Samaha, R. R., Gualerzi, C. & Noller, H. F. (1995). Specific protection of 16 S rRNA by translational initiation factors. *J. Mol. Biol.* **248**, 207-210.
- Moras, D., Dock, A. C., Dumas, P., Westhof, E., Romby, P., Ebel, J. P. & Giege, R. (1985). The structure of yeast tRNA(Asp). A model for tRNA interacting with messenger RNA. *J. Biomol. Struct. Dynam.* **3**, 479-493.
- Morosyuk, S. V., Lee, K.-S., SantaLucia, J., Jr & Cunningham, P. R. (2000). Structure and function of the conserved 690 hairpin in *Escherichia coli* 16 S ribosomal RNA: analysis of the stem nucleotides. *J. Mol. Biol.* **300**, 113-126.
- Morosyuk, S. V., SantaLucia, J., Jr & Cunningham, P. R. (2001). Structure and function of the conserved 690 hairpin in *Escherichia coli* 16 S ribosomal RNA. III. Functional analysis. *J. Mol. Biol.* **307**, 213-228.
- Mueller, F., Stark, H., van Heel, M., Rinke-Appel, J. & Brimacombe, R. (1997). A new model for the three-dimensional folding of *Escherichia coli* 16 S ribosomal RNA. III. The topography of the functional centre. *J. Mol. Biol.* **271**, 566-587.
- Mueller, F., Sommer, I., Baranov, P., Matadeen, R., Stoldt, M. & Wohnert, J. *et al.* (2000). The 3D arrangement of the 23 S and 5 S rRNA in the *Escherichia coli* 50 S ribosomal subunit based on a cryo-electron microscopic reconstruction at 7.5 Å resolution. *J. Mol. Biol.* **298**, 35-59.
- Muralikrishna, P. & Wickstrom, E. (1989). *Escherichia coli* initiation factor 3 protein binding to 30 S ribosomal subunits alters the accessibility of nucleotides within the conserved central region of 16 S rRNA. *Biochemistry*, **28**, 7505-7510.
- Nagaswamy, U., Voss, N., Zhang, Z. & Fox, G. E. (2000). Database of non-canonical base-pairs found in known RNA structures. *Nucl. Acids Res.* **28**, 375-376.
- Nikonowicz, E. P. & Pardi, A. (1992). Three-dimensional heteronuclear NMR studies of RNA. *Nature*, **355**, 184-186.
- Nikonowicz, E. P. & Pardi, A. (1993). An efficient procedure for assignment of the proton, carbon and nitrogen resonances in <sup>13</sup>C/<sup>15</sup>N-labeled nucleic acids. *J. Mol. Biol.* **232**, 1141-1156.
- Nikonowicz, E. P., Sirt, A., Legault, P., Jucker, F. M., Baer, L. M. & Pardi, A. (1992). Preparation of <sup>13</sup>C and <sup>15</sup>N-labelled RNAs for heteronuclear multidimensional NMR studies. *Nucl. Acids Res.* **20**, 4507-4513.
- Nikulin, A., Serganov, A., Ennifar, E., Tishchenko, S., Nevskaya, N. & Shepard, W. *et al.* (2000). Crystal structure of the S15-rRNA complex. *Nature Struct. Biol.* **7**, 273-277.
- Oehler, R., Polacek, N., Steiner, G. & Barta, A. (1997). Interaction of tetracycline with RNA: photoincorporation into ribosomal RNA of *Escherichia coli*. *Nucl. Acids Res.* **25**, 1219-1224.
- Osswald, M., Doring, T. & Brimacombe, R. (1995). The ribosomal neighborhood of the central fold of tRNA: cross-links from position 47 of tRNA located at the A, P or E site. *Nucl. Acids Res.* **23**, 4635-4641.
- Pardi, A. (1995). Multidimensional heteronuclear NMR experiments for structure determination of isotopically labeled RNA. *Methods Enzymol.* **261**, 350-380.
- Piotto, M., Saudek, V. & Sklenar, V. (1992). Gradient-tailored excitation for single-quantum NMR spectroscopy of aqueous solutions. *J. Biomol. NMR*, **2**, 661-665.
- Pley, H. W., Flaherty, K. M. & McKay, D. B. (1994a). Model for an RNA tertiary interaction from the structure of an intermolecular complex between a GAAA tetraloop and an RNA helix. *Nature*, **372**, 111-113.
- Pley, H. W., Flaherty, K. M. & McKay, D. B. (1994b). Three-dimensional structure of a hammerhead ribozyme. *Nature*, **372**, 68-74.
- Pon, C. L., Pawlik, R. T. & Gualerzi, C. (1982). The topographical localization of IF3 on *Escherichia coli* 30 S ribosomal subunits as a clue to its way of functioning. *FEBS Letters*, **137**, 163-167.
- Powers, T. & Noller, H. F. (1995). Hydroxyl radical footprinting of ribosomal proteins on 16 S rRNA. *RNA*, **1**, 194-209.

- Quigley, G. J. & Rich, A. (1976). Structural domains of transfer RNA molecules. *Science*, **194**, 796-806.
- Rinke-Appel, J., Junke, N., Osswald, M. & Brimacombe, R. (1995). The ribosomal environment of tRNA: crosslinks to rRNA from positions 8 and 20:1 in the central fold of tRNA located at the A, P, or E site. *RNA*, **1**, 1018-1028.
- SantaLucia, J., Jr & Turner, D. H. (1993). Structure of (rGGCGAGCC)<sub>2</sub> in solution from NMR and restrained molecular dynamics. *Biochemistry*, **32**, 12612-12623.
- Schlutzen, F., Tocilj, A., Zarivach, R., Harms, J., Gluehmann, M. & Janell, D. *et al.* (2000). Structure of functionally activated small ribosomal subunit at 3.3 angstroms resolution. *Cell*, **102**, 615-623.
- Schwalbe, H., Marino, J. P., King, G. C., Wechselberger, R., Bermel, W. & Griesinger, C. (1994). Determination of a complete set of coupling constants in <sup>13</sup>C-labeled oligonucleotides. *J. Biomol. NMR*, **4**, 631-644.
- Sklenar, V., Miyashiro, H., Zon, G., Miles, H. T. & Bax, A. (1986). Assignment of the <sup>31</sup>P and <sup>1</sup>H resonances in oligonucleotides by two-dimensional NMR spectroscopy. *FEBS Letters*, **208**, 94-98.
- Stallings, S. C. & Moore, P. B. (1997). The structure of an essential splicing element: stem loop IIa from yeast U2 snRNA. *Structure*, **5**, 1173-1185.
- Stark, H., Orlova, E. V., Rinke-Appel, J., Junke, N., Mueller, F. & Rodnina, M., *et al.* (1997). Arrangement of tRNAs in pre- and posttranslocational ribosomes revealed by electron cryomicroscopy. *Cell*, **88**, 19-28.
- Stern, S., Weiser, B. & Noller, H. F. (1988). Model for the three-dimensional folding of 16 S ribosomal RNA. *J. Mol. Biol.* **204**, 447-481.
- Stoffler-Meilicke, M. & Stoffler, G. (1987). The topography of ribosomal proteins on the surface of the 30S subunit of *Escherichia coli*. *Biochimie*, **69**, 1049-1064.
- Szewczak, A. A. & Moore, P. B. (1995). The sarcin/ricin loop, a modular RNA. *J. Mol. Biol.* **247**, 81-98.
- Szewczak, A. A., Kellogg, G. W. & Moore, P. B. (1993). Assignment of NH resonances in nucleic acids using natural abundance <sup>15</sup>N-<sup>1</sup>H correlation spectroscopy with spin-echo and gradient pulses. *FEBS Letters*, **327**, 261-264.
- Van de Peer, Y., Robbrecht, E., de Hoog, S., Caers, A., De Rijk, P. & De Wachter, R. (1999). Database on the structure of small subunit ribosomal RNA. *Nucl. Acids Res.* **27**, 179-183.
- Varani, G. & Tinoco, I., Jr (1991). RNA structure and NMR spectroscopy. *Quart. Rev. Biophys.* **24**, 479-532.
- Varani, G., Cheong, C. & Tinoco, I., Jr (1991). Structure of an unusually stable RNA hairpin. *Biochemistry*, **30**, 3280-3289.
- Varani, G., Aboul-ela, F. & Allain, H.-T. (1996). NMR investigation of RNA structure. *Prog. Nucl. Magn. Reson. Spectrosc.* **29**, 51-127.
- Wickstrom, E., Heus, H. A., Haasnoot, C. A. & van Knippenberg, P. H. (1986). Circular dichroism and 500-MHz proton magnetic resonance studies of the interaction of *Escherichia coli* translational initiation factor 3 protein with the 16 S ribosomal RNA 3' colacin fragment. *Biochemistry*, **25**, 2770-2777.
- Wimberly, B., Varani, G. & Tinoco, I., Jr (1993). The conformation of loop E of eukaryotic 5 S ribosomal RNA. *Biochemistry*, **32**, 1078-1087.
- Wimberly, B. T., Brodersen, D. E., Clemons, W. M., Jr, Morgan-Warren, R. J., Carter, A. P. & Vornrhein, C. *et al.* (2000). Structure of the 30 S ribosomal subunit. *Nature*, **407**, 327-339.
- Wollenzien, P., Expert-Bezancon, A. & Favre, A. (1991). Sites of contact of mRNA with 16 S rRNA and 23 S rRNA in the *Escherichia coli* ribosome. *Biochemistry*, **30**, 1788-1795.
- Woodcock, J., Moazed, D., Cannon, M., Davies, J. & Noller, H. F. (1991). Interaction of antibiotics with A- and P-site-specific bases in 16S ribosomal RNA. *EMBO J.* **10**, 3099-3103.
- Wyatt, J. R., Chastain, M. & Puglisi, J. D. (1991). Synthesis and purification of large amounts of RNA oligonucleotides. *Biotechniques*, **11**, 764-769.
- York, D. M., Darden, T. A. & Pedersen, L. G. (1993). The effect of long-range electrostatic interactions in simulations of macromolecular crystals—a comparison of the Ewald and truncated list methods. *J. Chem. Phys.* **99**, 8345-8348.

Edited by I. Tinoco

(Received 4 August 2000; received in revised form 29 November 2000; accepted 25 December 2000)



<http://www.academicpress.com/jmb>

Supplementary Material for this paper comprising six Tables with <sup>1</sup>H, <sup>13</sup>C, and <sup>31</sup>P chemical shift assignments, dihedral angles and CURVES helical parameters; ten Figures showing key portions of various 3D NMR spectra; and the complete NOE and dihedral angle restraint file is available from IDEAL.